

Cite this: *J. Mater. Chem. C*, 2017, 5, 5128

Macroscopically aligned nanowire arrays of π -conjugated polymers *via* shear-enhanced crystallization†

Jun-Huan Li,^{ab} Yuyin Xi,^{id c} Lilo D. Pozzo,^c Jun-Ting Xu^{id *a} and Christine K. Luscombe^{id *bd}

The nanoscale structure and macroscopic morphology of π -conjugated polymers are very important for their electronic application. While ordered single crystals of small molecules have been obtained *via* solution deposition, macroscopically aligned films of π -conjugated polymers deposited directly from solution have always required surface modification or complex pre-deposition processing of the solution. Here, ordered nanowires were obtained *via* shear-enhanced crystallization of π -conjugated polymers at the air–liquid–solid interface using simple deposition of the polymer solution onto an inclined substrate. The formation of macroscopically aligned nanowire arrays was found to be due to the synergy between intrinsic (π -conjugated backbone) and external (crystallization conditions) effects. The oriented nanowires showed remarkable improvement in the charge carrier mobility compared to spin-coated films as characterized in organic field-effect transistors (OFETs). Considering the simplicity and large-scale applicability, shear-enhanced crystallization of π -conjugated polymers provides a promising strategy to achieve high-performance polymer semiconductor films for electronics applications.

Received 3rd April 2017,
Accepted 11th May 2017

DOI: 10.1039/c7tc01419h

rsc.li/materials-c

Introduction

The flexibility and solution processability of π -conjugated polymers have stimulated considerable interest in their uses in various (opto)electronic devices for the past few decades.^{1–5} Many applications, however, require improvement in polymer semiconductor charge transport properties. The charge carrier mobility of solution-processed π -conjugated polymer films is generally limited by grain boundaries, trap sites and charge carrier hopping between polymer chains, leading to inefficient charge carrier transport.^{6–8} Charge carrier transport is expected to increase with improved control over the structural order, alignment and connectivity of polymer chains and crystals in thin films. While significant effort has been focused on the

chemical structure design and synthesis to control molecular ordering,^{9–12} the ways by which π -conjugated polymers are processed have an important effect on the device performance. Typical thin film deposition methods such as spin-coating, which can be used to produce wafer-scale homogeneous films (the diameter of the substrate can be as high as 30 cm), cannot be used to produce aligned nanowire morphologies. This is because the solvent evaporates rapidly during film formation providing kinetically unfavorable conditions for crystal growth.¹³ Achieving an ordered and oriented morphology for π -conjugated polymer thin films using solution-processing methods remains a key challenge.

Processing techniques such as treatment of the polymer containing solution prior to film deposition (*e.g.*, solution aging,¹⁴ sonication¹⁵ and UV irradiation^{16,17}), directional film deposition methods (*e.g.*, dip coating,¹⁸ zone casting,¹⁹ blade coating,²⁰ and shear coating^{21–23}) and post-deposition treatments (*e.g.*, rubbing^{24,25} and stretching²⁶) have proven to be effective strategies in controlling stacking and alignment of π -conjugated molecules. For instance, Yang *et al.* pretreated the conjugated polymer solution using ultrasonication to direct the self-assembly and extend the chain π -conjugation.²⁷ However, the above solution coating techniques are limited in their ability to align crystalline aggregates on a macroscopic scale. For example, ultrasonication facilitates chain stacking into crystals, but the crystals distribute randomly in the film.²⁷ To facilitate chain stacking and macroscopic alignment,

^a MOE Key Laboratory of Macromolecular Synthesis and Functionalization, Department of Polymer Science & Engineering, Zhejiang University, Hangzhou 310027, China. E-mail: xujt@zju.edu.cn

^b Materials Science & Engineering Department, University of Washington, Seattle, Washington 98195-2120, USA. E-mail: luscombe@uw.edu

^c Department of Chemical Engineering, University of Washington, Seattle, Washington 98195-1750, USA

^d Department of Chemistry, University of Washington, Seattle, Washington 98195-1700, USA

† Electronic supplementary information (ESI) available: Experimental details and characterization including TEM images of P3HT films prepared under different experimental conditions and 1D diffraction profiles extracted from 2D-GISAXS patterns. See DOI: 10.1039/c7tc01419h

it is often necessary to combine two or more techniques together,^{28,29} which inevitably requires multiple processing steps. For example, Reichmanis *et al.* aligned conjugated polymer nanowires by combining solution aging and UV irradiation to preform the nanowires in solution, followed by blade-coating to macroscopically align the nanowires.²⁸ In addition, the utility of solution coating methods is usually hampered by their specificity such as the need to have surface patterning,^{30,31} low-deposition speed³² and confined liquid flow.³³

Drop-casting on an inclined substrate is a simple and effective method of providing a directional shear force to align crystalline wires.^{34,35} The substrate is tilted, so that a drop line spreads down the substrate with a wedge shaped interface on the upper contact line. The crystal seeds tend to nucleate from the upper contact line and then crystals can orient in the crystal growth direction.³⁴ While drop casting of small conjugated molecules on an inclined substrate has resulted in well-controlled and aligned single-crystalline morphology,^{34–39} to our knowledge, there is only one report that has used the same technique to try and align π -conjugated polymers.⁴⁰

Our focus in this study was to enhance the molecular ordering of π -conjugated chains and orientation of nanowires in thin films using a one-step process. The solution containing P3HT was deposited onto an inclined substrate for the *in situ* formation of nanowire arrays. The alignment of nanowires and film morphology were systematically studied by means of transmission electron microscopy (TEM), atomic force microscopy (AFM) and optical microscopy (OM), while the chain ordering and molecular structure were further investigated by polarized ultraviolet-visible absorption spectroscopy (UV-vis) and grazing-incidence small-angle X-ray scattering (GI-SAXS). Furthermore, a clear correlation between the electrical properties and the alignment of nanowires was demonstrated through carrier mobility measurements. This work provides an extremely simple method for creating an ordered assembly of π -conjugated polymers into well-aligned arrays, thereby enhancing the charge carrier mobility.

Results and discussions

Alignment of polymer nanowires

The rigidity of the π -conjugated backbone and π - π interaction between chains contribute to the self-assembly of P3HT chains into crystalline nanowires.⁴¹ Simultaneously, the formation of highly ordered nanowires requires the polymer to have appropriate agility in solution to self-tune their chain conformation. In other words, the processing solvent for the polymer should impart suitable polymer chain mobility while having the ability to bundle the dissolved chains into crystals thereby facilitating molecular ordering.^{42,43} An important factor to aid in understanding the mobility of polymer chains in a solvent and its tendency to self-aggregate is to use Hansen solubility parameters (HSPs) (eqn (S2)–(S6) in ESI†). Here, ethyl benzoate (EB) was chosen to take advantage of suitable mobility of P3HT chains in this marginal solvent (Table S1 and Fig. S1, ESI†), based on the

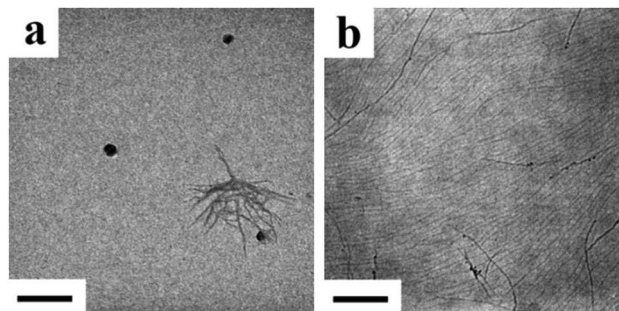


Fig. 1 TEM images of the films made by depositing (a) CB and (b) EB solution of LM-P3HT (0.3 mg mL^{-1}) on a horizontal substrate at room temperature ($25 \text{ }^\circ\text{C}$). Scale bar = 500 nm.

appropriate difference in HSPs for EB and P3HT, as revealed by the value of the relative energy difference (RED) ($\text{RED} \approx 1$).⁴⁴

To demonstrate the above idea, LM-P3HT (P3HTs with a low molecular weight of $M_n = 6.0 \times 10^3 \text{ g mol}^{-1}$, seen in Fig. S2 and S3, ESI†) was dissolved in its good solvent chlorobenzene (CB). The CB solution of P3HT was drop cast onto a horizontal substrate in a petri dish and then covered with a lid at room temperature. After the solvent evaporated completely, no ordered film structure was observed except some spherical or radial wire aggregates (Fig. 1a). This can be explained by the transfer of dissolved polymer from the contact line to the interior region as the solvent evaporates and contact line recedes from the periphery to the center of droplet.³⁶ P3HT chains dissolve well in CB and the solvent evaporation on the contact line fails to trigger the nucleation and growth of polymer nanowires. The mobile polymer chains in a good solvent are not able to stack into nanowires and only solidify into disordered aggregates after the remaining solvent evaporates.

When CB was replaced with EB, ordered nanowires were obtained (Fig. 1b). As the solvent evaporated, P3HT with limited chain mobility tended to stack into crystalline nanowires *via* intermolecular π - π interaction. These nanowires were locally oriented, which were formed with the aid of the air-liquid-solid interface.⁴⁵ Because the solution layer on the substrate was thin and the evaporation of the solvent was slow, the air-liquid-solid interface gradually receded and the nanowires grew along the receding direction. As the nuclei density is high at the air-liquid-solid interface,³⁶ the nanowires have a strong preference for growth along the moving direction of the solvent front of the three-phase interface.

With the aid of three-phase interface, the intermolecular π - π interaction and appropriate mobility of P3HT chains can promote the ordered bundle of loose chains into nanowires during crystallization. This idea can be further supported by modifying conditions to affect crystallization, such as concentration (Fig. S4, ESI†), temperature (Fig. S5, ESI†) and solvent evaporation rate (Fig. S6, ESI†). The morphological structure of crystalline domains can be altered by changing processing conditions because they influence the dynamic assembly process of π -conjugated polymers as they dry from a solution to form a solid thin film.⁴⁶ Through these studies, shown in detail in the ESI,† the best experimental conditions for locally ordered

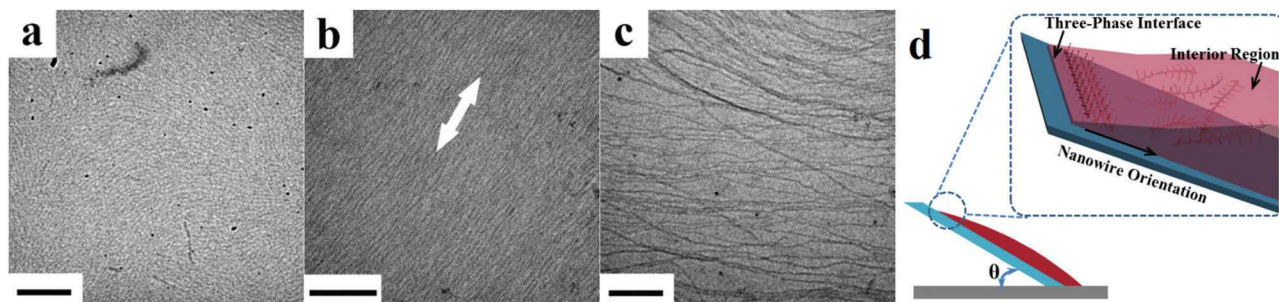


Fig. 2 TEM images of films made by depositing EB solution of LM-P3HT on the inclined substrate at (a) 60°, (b) 30° and (c) 10° angle. Scale bar = 200 nm. The white arrow in (b) indicates the nanowire orientation. (d) Schematic diagram of the inclined-substrate method.

nanowire growth were found to be drop-casting the EB solution of P3HT (0.3 mg mL^{-1}) at 25°C onto the horizontal substrate and then being kept in a covered petri dish.

As discussed in the introduction, the use of an external force during nanowire growth can facilitate the uniform orientation of nanowires on a macroscopic scale. Here, the substrate was inclined to provide this external force. When the inclined angle (θ) was large (e.g., 60°) (Fig. 2a), short and fractured nanowires formed in some areas. This unfavorable structure was caused by the rapidly retreating three-phase interface on the inclined substrate disturbing the continuous growth of nanowires. When θ was reduced to a smaller value such as 10° (Fig. 2c), the external force was not strong enough to direct the receding of the three-phase contact edge, causing the nanowire bundles to curve. When θ was 30° , the growth of nanowires was continuous and uniform with the nanowire alignment being perpendicular to the line of contact to the three-phase interface (Fig. 2b).

The crystallization of P3HT in the solvent can also be adjusted by changing the molecular weight of P3HT. The film became covered with entangled nanowires and then aggregates were formed as the molecular weight increased from $6.0 \times 10^3 \text{ g mol}^{-1}$, $2.0 \times 10^4 \text{ g mol}^{-1}$ to $3.2 \times 10^4 \text{ g mol}^{-1}$ (Fig. 2b and Fig. S7a and b, ESI†, respectively). This phenomenon was viewed as the deep trapping of kinetic structures caused by the lower solubility of HM-P3HT (P3HTs with a high molecular weight of $M_n = 2.0 \times 10^4 \text{ g mol}^{-1}$, seen in Fig. S8 and S9, ESI†) in EB. This further supports the idea that appropriate balance between intermolecular interaction and chain mobility is needed for the formation of macroscopically aligned nanowires. To monitor the

crystallization-assisted assembly process of HM-P3HT, a mixed solvent of EB and 1,2,4-trichlorobenzene (TCB) was applied, considering that TCB has closer HSPs with P3HT and slow evaporation rate similar to EB (Table S1, ESI†). It is also meaningful to explore the formation conditions of nanowire arrays with higher molecular weight of P3HT considering its better carrier transport characteristic.^{47,48} As shown in Fig. 3a, the use of the EB/TCB mixed solvent system gave rise to HM-P3HT films with obvious preferential alignment of nanowires with dense packing. In contrast, the spin-coated film appeared disordered with short nanowires and some random aggregates present as shown in Fig. 3b. The isotropic morphology of the spin-coated film proved the necessity of directional external force and three-phase interface for the formation of oriented nanowires.

To show the orientation of P3HT nanowires in a larger scale, optical microscopy (OM) was used (Fig. 4). The spin-coated film has no alignment feature (Fig. 4c and d). In contrast, the aligned films formed using the inclined substrate show oriented morphological feature as evidenced by the birefringence of the aligned film under crossed polarizers (Fig. 4b). The color change of the oriented film from blue under unpolarized light to yellowish under cross polarizers was completely different from that of spin-coated films from violet to completely black. This color variation indicates the parallel alignment and uniaxial orientation of nanowires within the polymer strips.⁴⁹ The morphological difference confirms the large-area alignment of the film *via* shear-enhanced crystallization compared to the isotropic film by spin-coating.

To probe the structural anisotropy of the P3HT nanowires, polarized UV-vis absorption spectra were measured (Fig. 5). All spectra exhibit the characteristic vibronic structure with three resolved transitions centered at 600 nm, 537 nm and 515 nm.²⁴ The characteristic dichroic ratio is defined as the ratio between absorption for perpendicular-polarized and parallel-polarized light relative to the nanowire orientation. The dichroic ratios at the above three wavelengths revealed the anisotropy of the oriented nanowire arrays, which coincided with the clear alignment feature as observed by AFM and OM. Since the π - π^* transition occurs along the P3HT backbone, the dipole vector for the light absorption of P3HT is parallel to the plane of polymer backbone.⁵⁰ As such, the absorption of UV light is the strongest when the electric vector of the incident light is parallel to the P3HT backbone or perpendicular to the nanowire.²⁶ As Fig. 5 shows, when the incident light was polarized in the

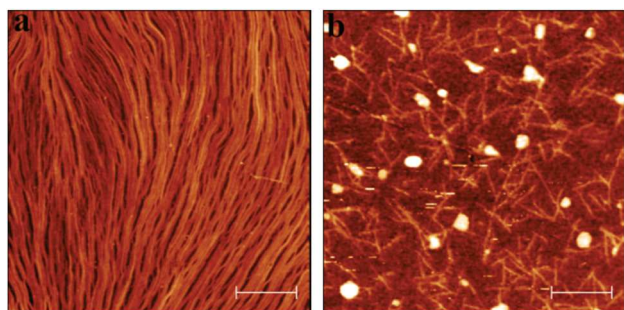


Fig. 3 AFM topological images of HM-P3HT films (a) made by depositing the mixed EB/TCB (2/1 v/v) solution on the inclined substrate at 30° angle and (b) made by spin coating. Scale bar = $1 \mu\text{m}$.

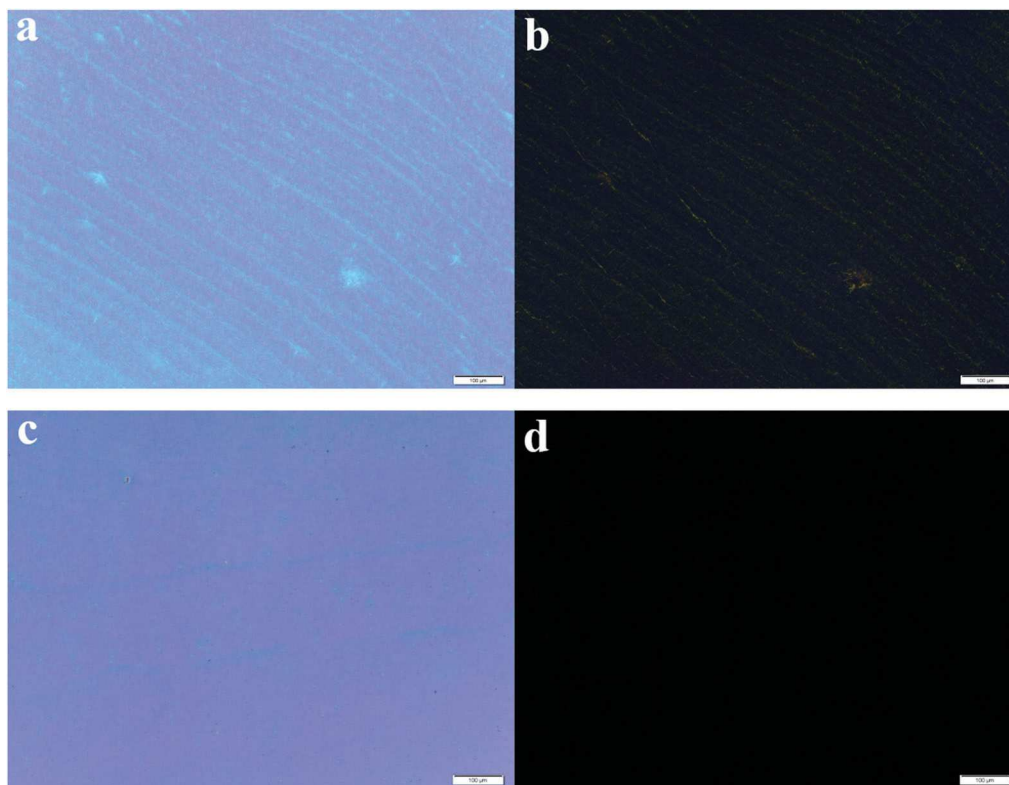


Fig. 4 OM images of HM-P3HT films formed by the inclined-substrate method under (a) unpolarized light or (b) crossed polarizers and spin-coated method under (c) unpolarized light or (d) crossed polarizers. Scale bar = 100 μm .

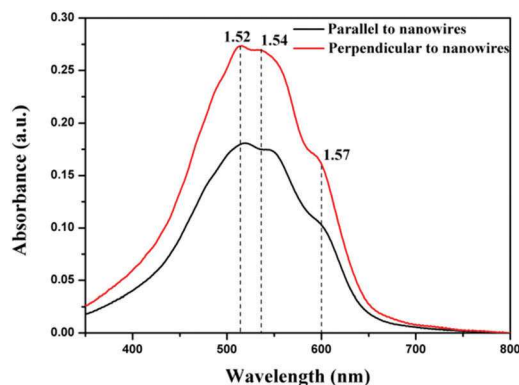


Fig. 5 Polarized UV-vis spectra of HM-P3HT nanowire array film polarized in the direction parallel (black) and perpendicular (red) to the nanowire orientation. The numerical values in the figure correspond to the measured dichroic ratios at three wavelengths.

direction perpendicular to the nanowire orientation, the light absorbance of nanowire arrays was stronger, compared to that of the polarized direction parallel to nanowire orientation. This indicates that the P3HT backbone is perpendicular to the nanowire orientation. Note that the dichroic ratio here is not very high despite the macroscopic nanowire alignment as shown in morphology characterization. We attribute this to the slight twisting of nanowires along the nanowire orientation (as seen in Fig. 3a), which may more or less disrupt the orientation of P3HT backbone within the film and thus decrease the dichroic ratio.^{24,50}

To provide further insight into the P3HT chain stacking behavior at the molecular level, grazing-incidence small-angle X-ray scattering (GI-SAXS) characterization was carried out (Fig. 6). The aligned film sample was measured with the incident X-ray beam both parallel (Fig. 6a) and perpendicular (Fig. 6b) to the nanowire orientation. In both directions, strong out-of-plane lamellar peaks (100) were observed (labeled with red dotted circles), corresponding to the repeat distance due to the alkyl chain lamellar stacking direction.⁵¹ The preferred out-of-plane scattering is indicative of an 'edge-on' orientation of P3HT chains.⁵² In contrast, the spin-coated film (Fig. 6c) shows a semicircle with a more uniform annular distribution (Fig. S10, ESI[†]), indicating that in this sample a number of crystallites are randomly oriented. Moreover, the lamellar peak (100) corresponding to the spin-coated sample is broader along the q_z direction (Fig. S10a, ESI[†]), due to the presence of more poorly ordered structure. Comparison of the preparation methods demonstrated improved molecular ordering for crystallization-assisted assembly of P3HT under inclined-substrate shearing. In summary, P3HT chains in films prepared *via* the inclined-substrate aligning method exhibit an 'edge-on' orientation and are also more organized than P3HT chains embedded within spin-coated films.

Field-effect mobility measurements

The charge transport properties of P3HT films deposited by spin-coating or by drop casting on an inclined substrate were investigated by fabricating organic field-effect transistors (OFETs) using a bottom-gate/up-contact geometry. Gold source/drain

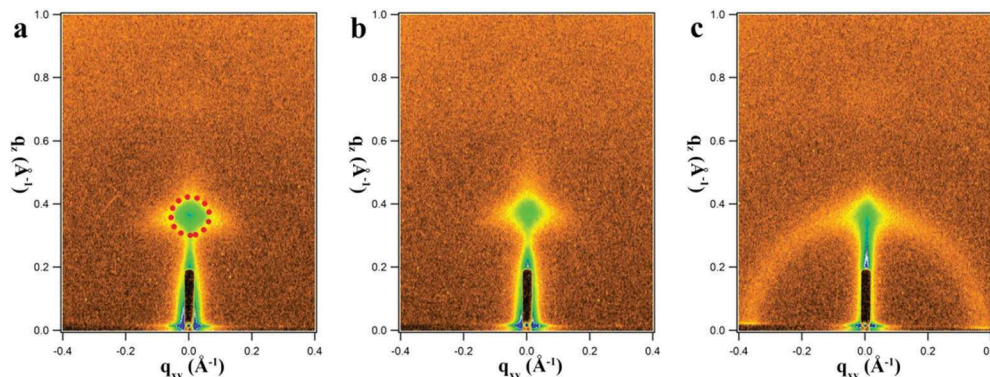


Fig. 6 GI-SAXS patterns of HM-P3HT films made by inclined-substrate method with incident X-ray (a) parallel and (b) perpendicular to the nanowire orientation and (c) made by spin-coating.

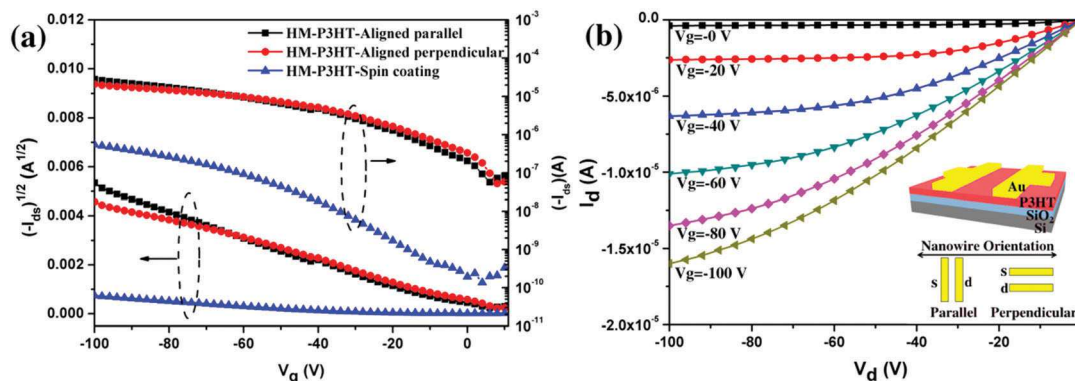


Fig. 7 (a) Typical transfer curves of HM-P3HT films made by inclined-substrate method with nanowire orientation parallel and perpendicular to the source–drain direction and made by spin-coating method. (b) Typical output curves of aligned P3HT films with nanowire orientation parallel to source–drain direction. Inset: An illustration of the direction of the source (s) and drain (d) electrodes relative to the nanowire orientation.

electrodes were patterned on top of deposited polymer film (transistor channel width = 1000 μm and length = 100 μm). The field-effect mobilities of aligned HM-P3HT films with nanowire orientation parallel and perpendicular to source–drain direction and spin-coated HM-P3HT films were measured. The transfer curves are shown in Fig. 7 and the mobilities are shown in Table 1 and Fig. S11 (ESI[†]). The aligned films showed an improvement in charge carrier mobility in both directions ($\mu_{\text{parallel}} = 0.01 \text{ cm}^2 \text{ V}^{-1} \text{ s}^{-1}$ and $\mu_{\text{perpendicular}} = 0.046 \text{ cm}^2 \text{ V}^{-1} \text{ s}^{-1}$) compared to spin-coated P3HT thin films ($\mu_{\text{spin-coating}} = 0.00320$). The improvement ($\mu_{\text{parallel}}/\mu_{\text{spin-coating}} = 31$, $\mu_{\text{perpendicular}}/\mu_{\text{spin-coating}} = 14$) can be attributed to the ordered stacking of P3HT chains and directional alignment of nanowires. The directional alignment

of crystalline nanowires, as well as the texture of P3HT aggregates, significantly influences the film mobility. The highest mobility of $0.126 \text{ cm}^2 \text{ V}^{-1} \text{ s}^{-1}$ was measured in an aligned HM-P3HT nanowire film, which corresponds to a 39-fold enhancement compared to the spin-coated films. Meanwhile, the close contact among the densely packing nanowire arrays accounted for the improvement of carrier mobility along the direction perpendicular to the source–drain electrodes. We anticipate that nanowires are interconnected with each other by tie-chain molecules. Due to the high carrier mobility in the direction of P3HT backbone, the nanowires aligned perpendicular to the channel still have better mobility than spin-coated films.^{26,28}

The molecular weight, OFET architecture and performance of P3HT from literatures are compared with the current work, as listed in the Table 2. Egap *et al.* aligned P3HT films by performing nanowires *via* UV irradiation and solution aging, and then shear coating the nanowires. The aligned films exhibited an average carrier mobility of $0.2 \text{ cm}^2 \text{ V}^{-1} \text{ s}^{-1}$ with a 33-fold enhancement compared to the spin-coated films.²¹ Reichmanis *et al.* macroscopically aligned P3HT nanowires by synergistically combing microfluidic shearing with UV irradiation. The average charge-carrier mobility reached $0.13 \text{ cm}^2 \text{ V}^{-1} \text{ s}^{-1}$ with an 11-fold enhancement compared with the spin-coated films.²³ Sung *et al.* combined inject printing and nanotransfer printing

Table 1 Average mobilities of HM-P3HT films made by different methods^a

Methods	Spin-coated	Inclined-substrate/perpendicular ^b	Inclined-substrate/parallel ^b
Mobility μ ($\text{cm}^2 \text{ V}^{-1} \text{ s}^{-1}$)	0.0032 ± 0.0003	0.046 ± 0.008	0.1 ± 0.02

^a Data are averaged over at least 15 devices for each condition and presented as average mobility \pm standard deviation. The detailed mobility distribution is shown in Fig. S11 (ESI). ^b Nanowire orientation with respect to the source–drain direction.

Table 2 Molecular weight, OFET performance and architecture of P3HT from literatures and current work

	M_n (g mol ⁻¹)	μ (cm ² V ⁻¹ s ⁻¹)	Improvement compared to the spin-coated films	Device architecture (channel length, width)
Egap <i>et al.</i>	9.0×10^4	0.2	33-fold	Bottom-contact/bottom-gate (50 μ m, 2000 μ m)
Reichmanis <i>et al.</i>	4.39×10^4	0.13	11-fold	Bottom-contact/bottom-gate (50 μ m, 2000 μ m)
Sung <i>et al.</i>	4.0×10^4	0.124	—	Top-contact/bottom-gate (80 μ m, 2 μ m)
Current work	2.0×10^4	0.10	31-fold	Top-contact/bottom-gate (100 μ m, 1000 μ m)

techniques to obtain large-scale nanowire arrays. The P3HT films exhibited a mobility of 0.124 cm² V⁻¹ s⁻¹.⁵³ All these studies need at least one complementary technique to enhance polymer alignment. In our study, the mobility of aligned P3HT films, while inferior to the state-of-the-art device performance, used an extremely simple one-step method of aligning conjugated polymer films *via* shear-enhanced crystallization to create the devices and thus is promising for future applications.

Conclusion

In conclusion, the three-phase interfacial assembly of π -conjugated P3HT chains into highly ordered nanowire arrays was obtained *via* simple deposition of the solution onto the inclined substrate as observed by TEM, AFM and OM. The experimental conditions affecting polymer crystallization, such as solvent, temperature, concentration, evaporation rate of solution, molecular weight and substrate-incline angle, were optimized to enhance the regularity of nanowire growth. The formation of well-aligned nanowire arrays is a synergy between intrinsic and external effects. Intrinsically, the polymer chains need to have backbone rigidity and strong intermolecular interaction, by which the polymer chains crystallize into nanowires. Extrinsically, the appropriate mobility of polymer chains in solution, three-phase interface and external force field are all key points regarding the formation of oriented arrays.

The P3HT chains stack into the nanowires with the backbone perpendicular to the nanowire orientation as revealed by polarized UV-vis. The nanowires grow as the contact line recedes, leading to the perpendicular orientation of nanowires to the contact line. Furthermore, based on GI-SAXS, P3HT chains in the oriented nanowires are mostly 'edge-on', with the alkyl chain lamellar perpendicular to the substrate. The oriented nanowire arrays have significant impact on the charge carrier mobility as characterized in FET devices with a 30–40 fold increase in mobility observed. Considering the simplicity and large-scale alignment, this assembly method of π -conjugated polymers possesses great potential in electronic applications.

Competing financial interest

The authors declare no competing financial interest.

Acknowledgements

This work was supported by National Natural Science Foundation of China (21574116) and NSF CHE-1506209 and DMR-1708317.

JHL thanks China Scholarship Council for financial support. The GISAXS measurement and analysis, performed by Y. Xi and L. D. Pozzo, was supported by Department of Energy Office of Basic Energy Sciences (DE-SC0010282).

References

- X. Guo, M. Baumgarten and K. Müllen, *Prog. Polym. Sci.*, 2013, **38**, 1832–1908.
- S. R. Forrest, *Nature*, 2004, **428**, 911–918.
- L. Dou, Y. Liu, Z. Hong, G. Li and Y. Yang, *Chem. Rev.*, 2015, **115**, 12633–12665.
- K. J. Baeg, M. Caironi and Y. Y. Noh, *Adv. Mater.*, 2013, **25**, 4210–4244.
- C. Wang, H. Dong, W. Hu, Y. Liu and D. Zhu, *Chem. Rev.*, 2012, **112**, 2208–2267.
- R. Noriega, J. Rivnay, K. Vandewal, F. P. V. Koch, N. Stingelin, P. Smith, M. F. Toney and A. Salleo, *Nat. Mater.*, 2013, **12**, 1038–1044.
- N. Kleinhenz, N. Persson, Z. Xue, P. H. Chu, G. Wang, Z. Yuan, M. A. McBride, D. Choi, M. A. Grover and E. Reichmanis, *Chem. Mater.*, 2016, **28**, 3905–3913.
- B. H. Smith, M. B. Clark, H. Kuang, C. Grieco, A. V. Larsen, C. Zhu, C. Wang, A. Hexemer, J. B. Asbury, M. J. Janik and E. D. Gomez, *Adv. Funct. Mater.*, 2015, **25**, 542–551.
- A. Takai, Z. Chen, X. Yu, N. Zhou, T. J. Marks and A. Facchetti, *Chem. Mater.*, 2016, **28**, 5772–5783.
- K. A. Mazzio, A. H. Rice, M. M. Durban and C. K. Luscombe, *J. Phys. Chem. C*, 2015, **119**, 14911–14918.
- Y. Wang, T. Hasegawa, H. Matsumoto, T. Mori and T. Michinobu, *Adv. Funct. Mater.*, 2017, **27**, 1604608.
- I. Kang, H. J. Yun, D. S. Chung, S. K. Kwon and Y. H. Kim, *J. Am. Chem. Soc.*, 2013, **135**, 14896–14899.
- F. C. Krebs, *Sol. Energy Mater. Sol. Cells*, 2009, **93**, 394–412.
- Y. D. Park, S. G. Lee, H. S. Lee, D. Kwak, D. H. Lee and K. Cho, *J. Mater. Chem.*, 2011, **21**, 2338–2343.
- D. Choi, M. Chang and E. Reichmanis, *Adv. Funct. Mater.*, 2015, **25**, 920–927.
- M. Chang, J. Lee, N. Kleinhenz, B. Fu and E. Reichmanis, *Adv. Funct. Mater.*, 2014, **24**, 4457–4465.
- A. R. Aiyar, J. I. Hong, R. Nambiar, D. M. Collard and E. Reichmanis, *Adv. Funct. Mater.*, 2011, **21**, 2652–2659.
- L. Li, P. Gao, K. C. Schuermann, S. Ostendorp, W. Wang, C. Du, Y. Lei, H. Fuchs, L. D. Cola, K. Müllen and L. Chi, *J. Am. Chem. Soc.*, 2010, **132**, 8807–8809.

- 19 C. M. Duffy, J. W. Andreasen, D. W. Breiby, M. M. Nielsen, M. Ando, T. Minakata and H. Sirringhaus, *Chem. Mater.*, 2008, **20**, 7252–7259.
- 20 M. R. Niazi, R. Li, M. Abdelsamie, K. Zhao, D. H. Anjum, M. M. Payne, J. Anthony, D. M. Smilgies and A. Amassian, *Adv. Funct. Mater.*, 2016, **26**, 2371–2378.
- 21 M. Chang, D. Choi and E. Egap, *ACS Appl. Mater. Interfaces*, 2016, **8**, 13484–13491.
- 22 L. Shaw, P. Hayoz, Y. Diao, J. A. Reinspach, J. W. F. To, M. F. Toney, R. T. Weitz and Z. Bao, *ACS Appl. Mater. Interfaces*, 2016, **8**, 9285–9296.
- 23 G. Wang, P. H. Chu, B. Fu, Z. He, N. Kleinhenz, Z. Yuan, Y. Mao, H. Wang and E. Reichmanis, *ACS Appl. Mater. Interfaces*, 2016, **8**, 24761–24772.
- 24 A. Hamidi-Sakr, L. Biniek, S. Fall and M. Brinkmann, *Adv. Funct. Mater.*, 2016, **26**, 408–420.
- 25 L. Hartmann, K. Tremel, S. Uttiya, E. Crossland, S. Ludwigs, N. Kayunkid, C. Vergnat and M. Brinkmann, *Adv. Funct. Mater.*, 2011, **21**, 4047–4057.
- 26 B. O'Connor, R. J. Kline, B. R. Conrad, L. J. Richter, D. Gundlach, M. F. Toney and D. M. DeLongchamp, *Adv. Funct. Mater.*, 2011, **21**, 3697–3705.
- 27 M. Lee, H. Jeon, M. Jang and H. Yang, *ACS Appl. Mater. Interfaces*, 2016, **8**, 4819–4827.
- 28 P. H. Chu, N. Kleinhenz, N. Persson, M. McBride, J. L. Hernandez, B. Fu, G. Zhang and E. Reichmanis, *Chem. Mater.*, 2016, **28**, 9099–9109.
- 29 N. E. Persson, P. H. Chu, M. McBride, M. Grover and E. Reichmanis, *Acc. Chem. Res.*, 2017, **50**, 932–942.
- 30 Y. Diao, B. C. K. Tee, G. Giri, J. Xu, D. H. Kim, H. A. Becerril, R. M. Stoltenberg, T. H. Lee, G. Xue, S. C. B. Mannsfeld and Z. Bao, *Nat. Mater.*, 2013, **12**, 665–671.
- 31 C. Luo, A. K. K. Kyaw, L. A. Perez, S. Patel, M. Wang, B. Grimm, G. C. Bazan, E. J. Kramer and A. J. Heeger, *Nano Lett.*, 2014, **14**, 2764–2771.
- 32 M. J. Lee, D. Gupta, N. Zhao, M. Heeney, I. McCulloch and H. Sirringhaus, *Adv. Funct. Mater.*, 2011, **21**, 932–940.
- 33 J. Shin, T. R. Hong, T. W. Lee, A. Kim, Y. H. Kim, M. J. Cho and D. H. Choi, *Adv. Mater.*, 2014, **26**, 6031–6035.
- 34 W. H. Lee, D. H. Kim, Y. Jang, J. H. Cho, M. Hwang, Y. D. Park, Y. H. Kim, J. I. Han and K. Cho, *Appl. Phys. Lett.*, 2007, **90**, 132106.
- 35 H. T. Yi, M. M. Payne, J. E. Anthony and V. Podzorov, *Nat. Commun.*, 2012, **3**, 1259.
- 36 J. A. Lim, H. S. Lee, W. H. Lee and K. Cho, *Adv. Funct. Mater.*, 2009, **19**, 1515–1525.
- 37 T. Uemura, Y. Hirose, M. Uno, K. Takimiya and J. Takeya, *Appl. Phys. Express*, 2009, **2**, 111501.
- 38 H. Li, B. C. K. Tee, J. J. Cha, Y. Cui, J. W. Chung, S. Y. Lee and Z. Bao, *J. Am. Chem. Soc.*, 2012, **134**, 2760–2765.
- 39 X. Zhang, J. Jie, W. Deng, Q. Shang, J. Wang, H. Wang, X. Chen and X. Zhang, *Adv. Mater.*, 2016, **28**, 2475–2503.
- 40 M. Trifunovic, T. Yokota, Y. Kato, T. Tokuhara, I. Hirata, I. Osaka, K. Takimiya, T. Sekitani, T. Someya and R. Ishihara, *19th International Workshop on Active-Matrix Flatpanel Displays and Devices (AM-FPD)*, Kyoto, Japan, 2012.
- 41 F. J. M. Hoeben, P. Jonkheijm, E. W. Meijer and A. P. H. J. Schenning, *Chem. Rev.*, 2005, **105**, 1491–1546.
- 42 N. Kleinhenz, C. Rosu, S. Chatterjee, M. Chang, K. Nayani, Z. Xue, E. Kim, J. Middlebrooks, P. S. Russo, J. O. Park, M. Srinivasarao and E. Reichmanis, *Chem. Mater.*, 2015, **27**, 2687–2694.
- 43 M. Chang, D. Choi, B. Fu and E. Reichmanis, *ACS Nano*, 2013, **7**, 5402–5413.
- 44 C. Panayiotou, *Hansen Solubility Parameters*, CRC Press, 2007, pp. 45–73.
- 45 U. Thiele, *Adv. Colloid Interface Sci.*, 2014, **206**, 399–413.
- 46 W. Shao, H. Dong, L. Jiang and W. Hu, *Chem. Sci.*, 2011, **2**, 590–600.
- 47 R. J. Kline, M. D. McGehee, E. N. Kadnikova, J. Liu and J. M. J. Fréchet, *Adv. Mater.*, 2003, **15**, 1519–1522.
- 48 F. P. V. Koch, J. Rivnay, S. Foster, C. Müller, J. M. Downing, E. Buchaca-Domingo, P. Westacott, L. Yu, M. Yuan, M. Baklar, Z. Fei, C. Luscombe, M. A. McLachlan, M. Heeney, G. Rumbles, C. Silva, A. Salleo, J. Nelson, P. Smith and N. Stingelin, *Prog. Polym. Sci.*, 2013, **38**, 1978–1989.
- 49 G. Lu, J. Chen, W. Xu, S. Li and X. Yang, *Adv. Funct. Mater.*, 2014, **24**, 4959–4968.
- 50 J. Liu, Y. Sun, X. Gao, R. Xing, L. Zheng, S. Wu, Y. Geng and Y. Han, *Langmuir*, 2011, **27**, 4212–4219.
- 51 H. Sirringhaus, P. J. Brown, R. H. Friend, M. M. Nielsen, K. Bechgaard, B. M. W. Langeveld-Voss, A. J. H. Spiering, R. A. J. Janssen, E. W. Meijer, P. Herwig and D. M. de Leeuw, *Nature*, 1999, **401**, 685–688.
- 52 S. Qu, Q. Yao, L. Wang, Z. Chen, K. Xu, H. Zeng, W. Shi, T. Zhang, C. Uher and L. Chen, *NPG Asia Mater.*, 2016, **8**, e292.
- 53 K. S. Park, J. Baek, Y. Park, L. Lee, Y. K. Lee, Y. Kang and M. M. Sung, *Adv. Mater.*, 2016, **28**, 2874–2880.